Electrophoretic microrheology of a dilute lamellar phase: Relaxation mechanisms in frequency-dependent mobility of nanometer-sized particles between soft membranes

Daisuke Mizuno,* Yasuyuki Kimura, and Reinosuke Hayakawa
Department of Applied Physics, Graduate School of Engineering, University of Tokyo, 7-3-1 Hongo, Bunkyo-ku, Tokyo 113-8656, Japan
(Received 18 April 2003; revised manuscript received 5 March 2004; published 30 July 2004)

Viscoelastic properties of complex fluids in the microscopic scale can be studied by measuring the transport properties of small, embedded probe particles. We have measured the complex electrophoretic mobility $\mu^*(\omega)$ of nanometer-sized particles dispersed in a lyotropic lamellar phase, which shows two relaxation processes at approximately 1 kHz (high frequency relaxation, HF) and 1 Hz (low frequency relaxation, LF). It is shown quantitatively that these processes are caused by the trapping of particles within two local structures of characteristic size in the lamellar phase: the interbilayer distance and the persistence length. The origin of observed relaxations is further investigated and augmented in this study with data obtained by two other complementary methods, dielectric spectroscopy and the direct observation of fluorescently labelled probe particles under an optical microscope. It is shown that the local distortion field of the lamellar phase is induced by the extra steric interaction involving the collision of a colloidal particle with the membrane. The resulting distortion field hinders the Brownian motion of colloidal particles parallel to the membranes (not vertical), and causes the observed HF relaxation. On the other hand, the origin of LF relaxation is presumably a result of the defects in the lamellar structure. Since the results of this study show that the transport property is strongly influenced by microscopic environments, this method is referred to as *electrophoretic microrheology*.

DOI: 10.1103/PhysRevE.70.011509 PACS number(s): 83.80.Qr, 82.70.−y, 87.16.Dg, 87.15.Tt

I. INTRODUCTION

The complex and hierarchical structure of soft materials such as gels, polymer solutions and micelles is one of the main factors attributing diverse functionality to these materials, especially in biological systems. The mechanical response of these materials is one of the most important and frequently studied properties, since it shows significant time or frequency dependence that reflects the innumerable kinds of interactions and transport phenomena associated with such complex structures. However, information given by a conventional rheometer (macrorheology) is not sufficient for the detailed investigation of the physics of soft materials since the data is averaged in macroscopic scales and the accessible frequency range cannot exceed 100 Hz due to the inertia of large samples and the apparatus.

The new research field of microrheology has recently been developed to overcome the inherent deficiencies of macrorheology [1–3]. Microrheology is not based on the stress-strain relation of matrices, but on the motion of small, embedded probe particles detected by several techniques such as particle tracking optical microscopy [4], laser interferometry [5,6] or dynamic light scattering [2]. Transport properties of probe particles measured by these techniques are transformed into an estimate of the viscoelasticity $\eta^*(\omega)$ of the surrounding matrix via the generalized Stokes-Einstein relation $D^*(\omega)=k_BT/6\pi\eta^*(\omega)a$, where k_B is the Boltzmann constant, D is a diffusion constant, and a represents the radius of particles. Hereafter, a parameter shown with an asterisk indicates that the parameter is of complex quantity. In this respect, the spatial scale of microrheology reduces to the size of the probe particles, and the available frequency can be extended to the MHz range [7]. However, since the minimum size of a probe particle is usually limited by the diffraction of light or the intense scattering from the bulk media, probe particles are normally larger than the characteristic length of the matrix, such as the mesh size of a gel network.

The complex electrophoretic mobility $\mu^*(\omega)$ of colloidal particles is measured in this study using a method recently developed in our laboratory [8,9]. Complex electrophoretic mobility is a frequency dependent response function of velocity to the sinusoidal electric field. The extreme sensitivity of our method and the ability to remove attendant noise allows the use of nanometer-sized colloids as probe particles, which are smaller than the characteristic length of the surrounding material. In such a case, the change of mobility provides more information [1] on local structures and local interactions between particles and the surrounding materials, than that obtained by continuum viscoelasticity measured with larger probes.

This method of electrophoretic microrheology is applied to a lyotropic lamellar phase composed of surfactant bilayers. Even in this simple system, there are hierarchical structures as shown in Fig. 1 [10]. A lyotropic lamellar phase is made of alternative stacks of solvent and bilayer membranes with an intermembrane distance d. The stability of the periodical lamellar structure is considered a derivation of the steric interactions between fluctuating and colliding membranes.Therefore, the length between colliding points l is also an important length scale. Lamellar phase loses orientational order at a length scale longer than L, and three-dimensional packing of crumpled membranes needs topological defects, which may also slowly fluctuate with time according to generation and annihilation.

*Electronic address: dsmizuno@nat.vu.nl; Present address: Division of Physics and Astronomy, Faculty of Sciences, Vrije Universiteit, Amsterdam, De Boelelaan 1081, 1081 HV Amsterdam.

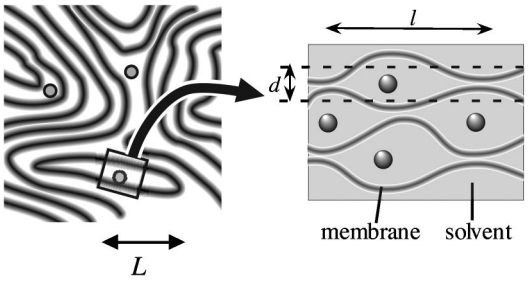

FIG. 1. Schematics of probe particles dispersed in a lyotropic lamellar phase with layer distance d. The length L is the correlation length of the orientational order of membranes and l is the longest wavelength of the free fluctuation of a membrane.

The observed spectrum of $\mu^*(\omega)$ reveals two relaxation processes at approximately 1 kHz (high frequency relaxation, HF) and 1 Hz (low frequency relaxation, LF) [11]. The typical length scale of each relaxation is in quantitative agreement with the size of the two characteristic local structures of the lamellar phase. The potential size of the HF relaxation corresponds to the interbilayer distance d, and that of the LF mode to persistence length L. In order to further investigate the mechanism of observed relaxations, we performed two additional complementary experiments: dielectric response spectroscopy and the direct observation of the motion of fluorescently labelled probe particles. The dielectric spectrum indicates that the Maxwell-Wagner relaxation caused by the lamellar structure is located at a frequency higher than that associated with HF relaxation. [12] This means that the electric field working on particles is parallel to the membrane in the frequency range used to measure $\mu^*(\omega)$. We therefore conclude that the HF relaxation mode originates from the hindrance of diffusion of colloidal particles parallel to membranes, not vertical to membranes.

This study has theoretically shown that the local distortion field [13] of the lamellar phase is induced by the collision of a colloidal particle with membranes. The resulting distortion field hinders the Brownian motion of colloidal particles parallel to membranes. The dynamics of such a particle-distortion pair is discussed in detail, and it is discovered that the theoretical prediction coincides well with the observed spectrum $\mu^*(\omega)$.

On the other hand, the detailed mechanism of LF relaxation is not clear, although it is assumed to be caused by defect structures of the lamellar phase, such as multibilayer vesicles and onions. That is partly because $\mu^*(\omega)$ completely relaxes at frequencies below the LF mode and DC mobility is not available. The existence of LF relaxation is confirmed in this study by the direct observation of the motion of colloidal particles under an optical microscope. Colloidal particles are normally trapped in one particular location for several seconds and sometimes hop to another site. The relaxation time obtained from the evolution of mean-squared displacement was consistent with the LF relaxation time in $\mu^*(\omega)$. Certain trajectories of colloidal particles possess a particular path of connecting trapping sites, and which is sometimes renewed instantly. Therefore, the mechanism of the LF relaxation mode is supposedly influenced by dynamic disorder transport [14] between defect structures of the lamellar phase.

II. METHODS

A. Wide-band spectroscopy of complex electrophoretic mobility $\mu^*(\omega)$

Colloidal particles in suspension are usually charged due to the desorption or adsorption of low molecular ions, and therefore move toward the direction of the external electric field (electrophoresis). DC electrophoretic mobility μ_{dc} is determined as a ratio of the velocity of colloidal particles to the DC applied electric field. When an AC electric field is applied, electrophoretic mobility is generally given as a frequency-dependent complex response function $\mu^*(\omega) = \mu \exp(i\delta)$, which is expected to yield more information than that supplied by DC electrophoresis [15]. We have recently developed a new method for measuring complex electrophoretic mobility $\mu^*(\omega)$ with the heterodyne technique of dynamic light scattering under a sinusoidal electric field $E_0 \cos \omega t$.

The heterodyne technique of dynamic light scattering uses a coherent laser light as a probe, and light scattered from the sample is detected by mixing with a reference light. The phase of the scattered light shifts by the difference relative to the optical path $\mathbf{q}\cdot\delta\mathbf{r}$ due to the displacement $\delta\mathbf{r}$ of a colloidal particle, where $\mathbf{q}$ is a scattering wave vector. The scattered light detected with the heterodyne method results in a signal that is proportional to $\cos(\mathbf{q}\cdot\delta\mathbf{r})$. Since displacement of a colloidal particle is the sum of the displacement due to Brownian motion $\delta\mathbf{r}_0$ and that due to electrophoresis $\delta\mathbf{r}_E = \mu\mathbf{E}_0 \sin(\omega t+\delta)/\omega$, the signal intensity under a small electric field is written as

$$\cos[\mathbf{q}\cdot(\delta\mathbf{r}_0+\delta\mathbf{r}_E)] \sim \cos(\mathbf{q}\cdot\delta\mathbf{r}_0) - \frac{\mu(\mathbf{q}\cdot\mathbf{E}_0)\sin(\delta\mathbf{q}\cdot\mathbf{r})}{\omega}\sin(\omega t+\delta) \equiv \cos(\mathbf{q}\cdot\delta\mathbf{r}_0)+A_1(\omega), \quad (1)$$

where $\mathbf{E}_0$ is the amplitude of the applied electric field. It is worth noting that the amplitude of A_1, defined by $\mu(\mathbf{q}\cdot\mathbf{E}_0)\sin(\mathbf{q}\cdot\delta\mathbf{r}_0)/\omega$, is a random variable with an average value of zero. Therefore, the detection of a second harmonic frequency component A_1' obtainable by squaring A_1 allows the derivation of $\mu^*(\omega)$ from Eq. (1). Further detailed principles pertaining to this method are discussed in Appendix A and within previous publications [8,9].

The experimental setup used in this study is shown in Fig. 2. Incident laser light (He-Ne, $\lambda = 6328$ Å) is crossed with reference light in a cylindrical sample cell in order to facilitate the detection of light with the heterodyne method [16]. The scattering wave number determined by the crossing angle ($\theta = 10°$) is $q = 2.3\times10^6$ m^{-1}. In the sample cell, parallel plate platinum electrodes are separated by a distance of 5 mm. The sinusoidal electric field generated by a synthesizer (HP33120A) is amplified with a high-voltage amplifier (PA84) and applied to the sample. The scattered light mixed with the transmitted reference light is detected with the optical heterodyne technique and amplified with a preamplifier (AD624). The harmonic frequency component of the applied electric field in the detected signal is extracted by using a

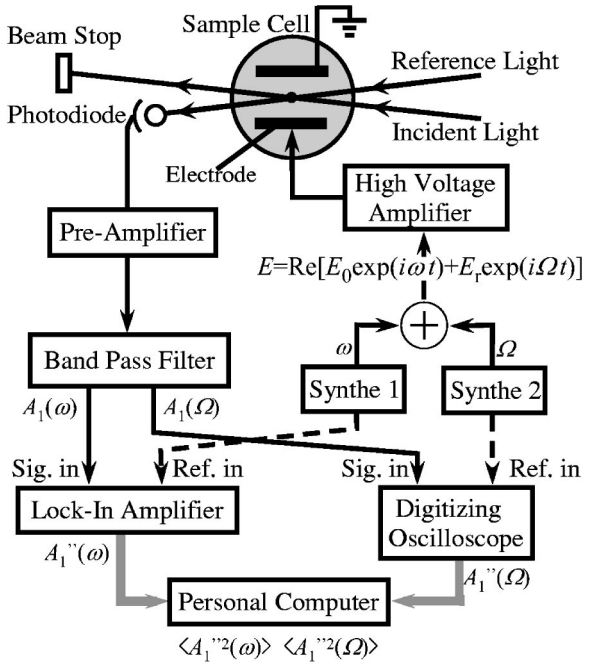

FIG. 2. Schematic diagram of the experimental setup for wide-band spectroscopy of complex electrophoretic mobility.

band-pass filter (NF3628). In previous studies [8,9] the filtered signal is squared with an analog multiplier before being detected with a lock-in amplifier (SR830) because the correlation time of $\sin(\mathbf{q}\cdot\delta\mathbf{r}_0)$ in Eq. (1) is much faster than the time constant t_c of the lock-in amplifier. In this study, however, the Brownian motion of probe particles dispersed in a lamellar structure is so slow that the signal A_1 can be detected with a lock-in amplifier beforehand, and the output of the lock-in amplifier $A_1''=\mu(\mathbf{q}\cdot\mathbf{E}_0)\sin(\mathbf{q}\cdot\delta\mathbf{r}_0)\exp\{i(\delta-\pi/2)\}/\omega$ is then digitally squared as a complex quantity to obtain $\langle A_1''^2\rangle$ on a personal computer. As indicated in Appendix A, the first and second order harmonic signal is measured at 230 Hz to measure the magnitude of complex electrophoretic mobility. $\mu^*(\omega)$ for an arbitrary frequency ω is obtained by comparing $\langle A_1''^2\rangle(230\ \mathrm{Hz})$ and $\langle A_1''^2\rangle(\omega)$. In order to calibrate the temporal change of measurement efficiency, we applied the sum of the electric field with the frequency of ω and 230 Hz. An extra phase shift or change of amplitude due to the devices,such as the filter and the multiplier, is corrected by measuring the reference signal instead of the detected signal.

B. Electrophoretic microrheology

We measured $\mu^*(\omega)$ of colloidal particles dispersed in a complex fluid to study local mechanical properties. Usually, DC electrophoretic mobility is simply related to the surface potential of colloidal particles via the Smoluchowski equation $u=\varepsilon\zeta/\eta$, where ζ is the zeta potential of colloidal surface, ε and η are the permittivity and DC viscosity of the surrounding solvent. The Smoluchowski equation is simply extended to the frequency-dependent case as $\mu^*(\omega)=\varepsilon\zeta/\eta^*(\omega)$ when the intrinsic mobility of a probe particle is independent of frequency. In this study, intrinsic mobility refers to the mobility of a particle in water, which is usually independent of frequency in the absence of certain particular situations [8,9]. Therefore, $\mu^*(\omega)$ offers information on the local viscoelastic property $\eta^*(\omega)$ of the solvent surrounding the particle.

Since the applied electric field does not induce translational motion of the surrounding bulk media, information on $\mu^*(\omega)$ of the probe particles can be extracted even under intense background scattering. This is a distinct advantage of our method, and it enables us to use nanometer-sized particles that are smaller than the characteristic length of bulk media (intermembrane distance d of the lyotropic lamellar phase in this study). Therefore, μ^* or η^* measured by electrophoretic microrheology reflects the mesoscopic structure of complex fluids or the microscopic circumstances of probe particles, where the assumption of continuum viscoelasticity might be broken [1].

C. Particle tracking fluorescent microscopy

Colloidal particles smaller than the wavelength of visible light cannot be directly observed under a regular optical microscope. But we can trace the motion of small particles by labeling them with fluorescent dye. In this study, the motion of fluorescent colloidal particles (diameter $2a=57$ nm, Polysciences, Inc.) in a lamellar structure was observed directly with a fluorescence microscope (TE300, Nikon). A sample is filled in a laboratory dish with a cover slip at its bottom, and sealed with a cover glass. The observed image of a particle was detected with a CCD camera (Tokyo Inst.) and image contrast was digitally enhanced with Argus20 (Hamamatsu). The time resolution of the measurement is limited by the video frequency (30 Hz). We evaluated the center of gravity of a particle $\mathbf{r}_c$ from the captured digital image by weighting its digitized intensity. The use of this procedure allows the resolution of a particle's position to improve by 1/10 of a pixel (about 10 nm).

This method can provide information on transport properties of colloidal particles that complements the measurement of complex electrophoretic mobility $\mu^*(\omega)$ because the time evolution of the mean-squared displacement calculated from $\mathbf{r}_c(t)$ is directly related to $\mu^*(\omega)$ with the classical linear response theory [17] as

$$\mu^*(\omega)=\frac{Q_eD^*(\omega)}{k_BT}=-\frac{Q_e}{4k_BT}\omega^2\int_0^\infty dt\,\exp(-i\omega t)\langle[\mathbf{r}_c(t)-\mathbf{r}_c(0)]^2\rangle, \tag{2}$$

where Q_e is an effective charge of a colloidal particle.

D. Dielectric relaxation spectroscopy

The dielectric response of the lyotropic lamellar phase including colloidal particles was measured with changing temperature or concentration of surfactants and colloidal particles. Samples were left to rest for sufficient time before

measurement to allow equilibrium and the stabilization of temperature [12]. The complex impedance Z_s^* of the sample set in a temperature-controlled cylindrical cell was measured by an LF impedance analyzer (HP4192A) in the frequency range 10 Hz to 13 MHz. The parallel plate electrodes are made of platinum coated with platinum black. The area S_0 and distance between electrodes d_0 are, respectively, 4.5 cm^2 and 5 mm. The cell constant of the parallel plate electrodes, determined by measuring the capacitance of several liquids with known permittivity, was estimated at 8.9 m^{-1}. This value is confirmed prior to the commencement of each experiment by obtaining a measurement using pure distilled water. The measured impedance Z_s^* was analyzed by regarding the sample as a parallel circuit of frequency-dependent capacitance $C_s(\omega)$ and conductance $G_s(\omega)$.

III. MATERIALS

The sample surfactant solution is a ternary mixture of *n*-dodecyl pentaethyleneglycol monododecylether ($C_{12}E_5$)/1-hexanol/water [18,19] to which was added polystyrene latex particles with diameter of $2a=42$ nm (Dow. Co. Ltd.). In the case of fluorescent microscopy, latex particles with $2a=57$ nm (Polysciences, Inc.) were used instead. The lamellar phase in this system swells up with very small amounts of surfactants. The measured value of membrane thickness δ_m is 3 nm [18]. An interbilayer spacing d is obtained from the simple swelling law of lyotropic lamellar phase, $d \sim \delta_m/\phi_m$. Here, the volume fraction ϕ_m of the bilayer membrane made up of $C_{12}E_5$ and hexanol is determined by taking into account the solubility of hexanol in water ($\sim 0.3\%$).

A sample is prepared in the concentration range $0.02 < \phi_m < 0.06$ (130 nm $> d >$ 50 nm) to satisfy the relation $d > 2a$ so that the colloidal particles are homogeneously dispersed between membranes. The total amount of latex particles (about 0.1 wt.% or less) added to the lamellar sample is small enough to satisfy the condition $n_c \ll 1/d^3$, where n_c is the number density of colloidal particles. The interaction between particles is therefore negligible in such a dilute dispersion. It has been confirmed that the colloidal particles are homogeneously dispersed between membranes, and the phase diagram is not affected by the inclusion of latex particles if their concentration is less than a few wt.% and the intermembrane distance is larger than the particle size [20,21]. However, the phase behavior of the sample was confirmed on each occasion with dielectric spectroscopy [12]. Since the amplitude of the displacement of a particle due to electrophoresis is much less than d, it has little influence on the lamellar structure. Unless indicated otherwise, all experiments are conducted within a specific room temperature range (26°C–28°C).

IV. RESULTS

A. Complex electrophoretic mobility of probe particles dispersed in the lamellar phase

Figure 3 shows the mobility $\mu^*(\omega)$ of latex particles dispersed in the aqueous phase of $C_{12}E_5$ at CMC and 0.3 wt% hexanol. This chemical composition is almost the same as

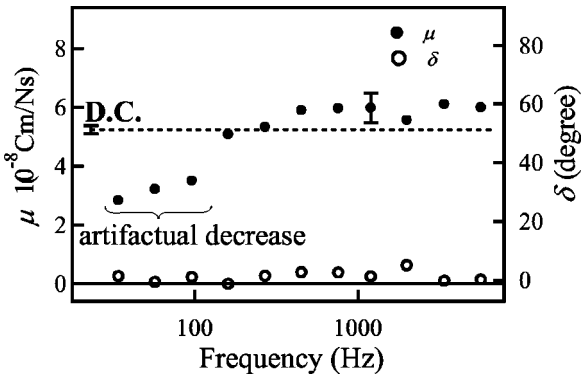

FIG. 3. Frequency dependence of complex electrophoretic mobility $\mu^* = \mu e^{i\delta}$ of latex particles dispersed in an aqueous phase of $C_{12}E_5$ at CMC and hexanol at a saturated concentration (0.3 wt%). Broken line shows the value of DC electrophoretic mobility ($\mu_{dc} = 5.7 \times 10^{-8}$ Nm/Cs) measured with ELS-800. See text for an explanation of the artifactual decrease in magnitude μ observed at low frequencies.

that of the aqueous phase between membranes of a lyotropic lamellar solution. A decrease in magnitude μ observed at frequencies lower than 100 Hz is considered an artifact since there is no phase shift in the same frequency range. The reason for this apparent decrease was explained in our previous papers. Frequency dispersion of each harmonic frequency component of the detected signal is very broad for our sample due to the fast Brownian motion of very small latex particles. Since the bandwidth of the electric filter used in this study is proportional to the center frequency, the entire signal cannot pass through the filter at low frequencies. The broken line in Fig. 3 shows the value of DC electrophoretic mobility measured with ELS-800 (Otsuka elec.), $\mu_{dc} = 5.7 \times 10^{-8}$ nm/Cs, which is in good agreement with the magnitude of mobility in the higher frequency region. It is therefore confirmed that there is no relaxation for the electrophoretic mobility of probe particles in this measured frequency range, and the local rheological environment is safely obtained from $\mu^*(\omega)$.

Figure 4(a) shows the frequency dependence of μ^* obtained in a lamellar phase at $\phi_m = 4.7\%$. There are two relaxations in the spectrum, and the relaxation frequencies are, respectively, named f_L and f_H. We divide the frequencyspectrum into three respective regions by f_L and f_H to yield region I, II, and III. Hereafter, the values for the mobility μ, diffusion coefficient D and drag coefficient γ at the plateau in respective regions are denoted by the subscript I, II, and III. The solid lines in Fig. 4 are the best-fit curves of the sum of two relaxation spectra with the relaxation time $\tau_L (=1/2\pi f_L)$ and $\tau_H (=1/2\pi f_H)$,

$$\mu^*(\omega) = (\mu_{III} - \mu_{II}) \frac{i\omega\tau_H}{1 + i\omega\tau_H} + \mu_{II} \frac{i\omega\tau_L}{1 + i\omega\tau_L}, \qquad (3)$$

where $\tau_H = 1.7 \times 10^{-4}$s, $\tau_L = 6.6 \times 10^{-2}$s, $\mu_{III} = 1.5 \times 10^{-8}$ cm/Ns and $\mu_{II} = 9.2 \times 10^{-9}$ cm/Ns. The mobility μ_{III} and μ_{II} are considerably smaller than μ_0 measured in an aqueous phase without a lamellar structure.

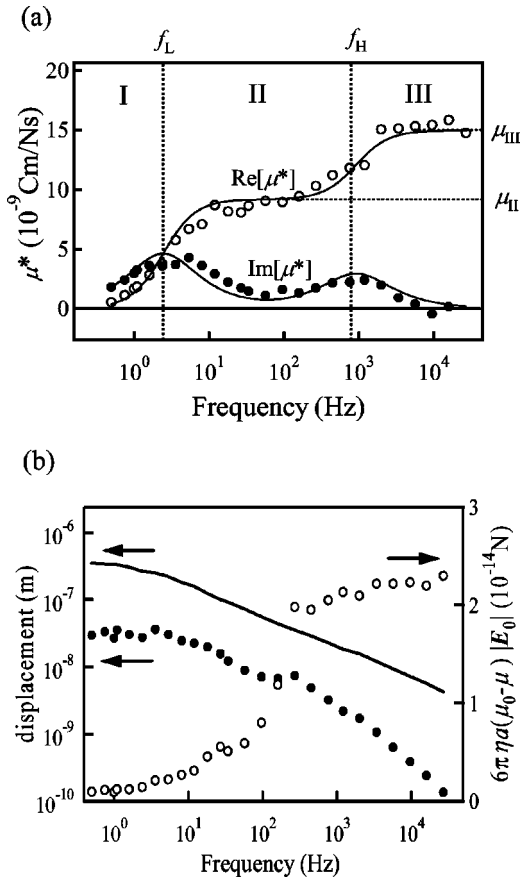

FIG. 4. (a) Frequency dependence of complex electrophoretic mobility μ^* of latex particles dispersed in a nonionic lamellar phase of $C_{12}E_5$/hexanol/water system (ϕ_m=4.7%). The solid lines are best-fit curves of Eq. (3). Errors of the measured values are about 5–8 %. (b) Comparison of electrophoretic motion (filled circles) and Brownian motion (solid line), and estimation of force applied to membranes by one particle (open circles).

Since there is enough free space for an electric double layer around probe particles, it is assumed that electrokinetic properties of the latex particles are not influenced by the presence of membranes. Therefore, the observed frequency dependence of $u^*(\omega)$ is a result of microscopic interactions between probe particles and membrane structures. An explanation of the strength of perturbation of the membrane-particle interaction due to electrophoretic motion follows. The average amplitude of electrophoretic motion, indicated by filled circles in Fig. 4(b), is calculated as $\mu|\mathbf{E}_0|/\omega$. In this measurement, a small electric field is carefully applied to the sample, and the linear relation between the amplitude and applied field is confirmed at several frequencies. Therefore, electrophoretic motion is always smaller than thermal Brownian motion, which is estimated as $\sqrt{D(\omega)/\omega} = \sqrt{\mu(\omega)k_BT/6\pi\mu_0\eta a\omega}$ and shown as a solid curve in Fig. 4(b). The perturbation force applied to membranes by the electrophoretic motion of each particle, shown as open circles in Fig. 4(b), is estimated as $6\pi\eta a(\mu_0-\mu)|\mathbf{E}_0|$. It is revealed that the interaction energy, estimated simply as the product of the amplitude and force, is much smaller than the thermal energy k_BT. Therefore, it is clear that the membrane structure is not influenced strongly by the electrophoretic motion of the colloidal particles.

TABLE I. Volume fractions of each component in samples used in this study, and intermembrane distance estimated using the simple swelling law.

$C_{12}E_5$(%)	Hexanol (%)	ϕ_m(%)	d(nm)
2	0.650	2.35	123
2	0.730	2.43	128
2.5	0.750	2.95	102
3	0.852	3.55	85
3.5	0.946	4.15	72
4	1.04	4.74	63
5	1.20	5.90	51

Now, the observed frequency dependence of $\mu^*(\omega)$ is discussed by assuming that colloidal particles are under the potential barrier caused by the interaction with lamellar structures. In this case, the relaxation time τ is estimated from thetime required for a particle to diffuse the length of thermal fluctuation $\Lambda_{H(L)}$, which is the typical size of the potential barrier estimated from the thermal energy $\sim k_BT$. The relaxation times $\tau_{H(L)}$ are written as

$$\tau_{H(L)} \sim \Lambda^2_{H(L)}/2D_{III(II)} = \gamma_{III(II)}\Lambda^2_{H(L)}/2k_BT, \tag{4}$$

where $\Lambda_{H(L)}$ is the amplitude of fluctuation of probe particles in the potential barrier for HF (LF) relaxation. The drag coefficients γ_{III} and γ_{II} can be determined from the measured mobility by

$$\gamma_{III(II)} = 6\pi\eta_0 a\mu_0/\mu_{III(II)}, \tag{5}$$

where η_0 and μ_0 are the viscosity of water and electrophoretic mobility in the aqueous phase, respectively. We can estimate the size Λ of the potential barrier as

$$\Lambda \sim \sqrt{2k_BT\tau/\gamma}, \tag{6}$$

which is 33 nm for HF relaxation and 500 nm for LF relaxation at ϕ_m=4.7%. Measurement conditions and estimations of $\Lambda_{H(L)}$ for all samples are listed in Table I and Fig. 5, respectively.

As we mentioned previously, there are three characteristic length scales in a lamellar phase composed of a nonionic surfactant, as schematically shown in Fig. 1 [6]. The intermembrane distance d, mean distance l between the points where a membrane collides with its neighboring membranes, and the persistent length of the orientational order L. The length l is roughly estimated as $l \sim \sqrt{4\pi^3 k_c/\Xi k_BTd}$ [10], where k_c is the mean curvature elasticity of a single membrane and Ξ is a constraining parameter estimated as 0.1–0.2 from simulations [22] and the measurement of intermembrane interactions [23]. On the other hand, L is estimated as $L \sim \beta \exp(2\pi k_c/k_BT)$ [10], where β is a short-distance cutoff of the order of a molecular length. In the sample we studied, we can estimate $l=4d-7d$ and $L \sim 500$ nm when using the reported value of $k_c \sim 0.8k_BT$ [18]

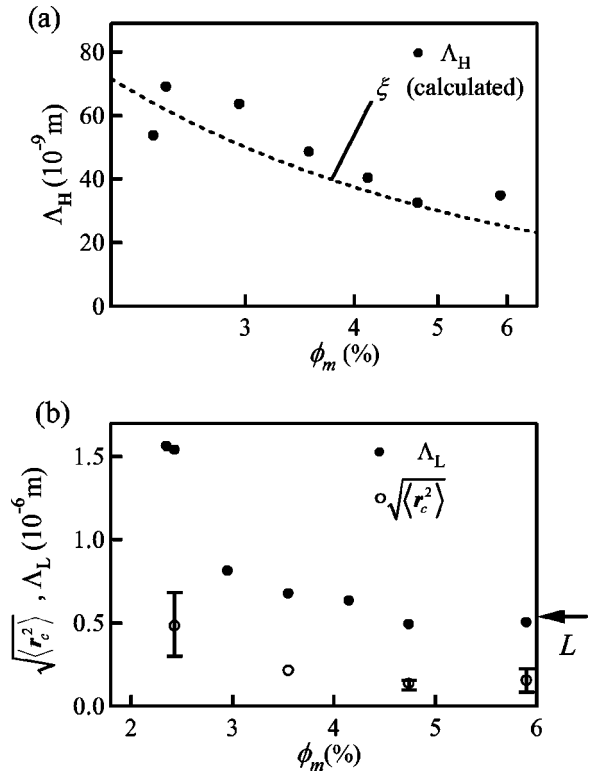

FIG. 5. Comparison of characteristic length for (a) HF relaxation (Λ_H, ξ) and (b) LF relaxation $(\Lambda_L, \sqrt{\langle \mathbf{r}_2^c \rangle})$.

and assume β to be δ_m. Therefore, two characteristic lengths of the potential barrier estimated from the experiment are found to correspond to the characteristic size of the lamellar structure $\xi \equiv d/2$ ($\sim$32 nm at $\phi_m = 4.7\%$) and L as shown in Fig. 5. This means that the potential barrier formed by flexible membranes traps colloidal particles within these length scales. It is noted that ξ is a reasonable estimation for Λ_H.

Figure 6 qualitatively illustrates the mechanism of the observed relaxations. At the highest frequencies of region III, colloidal particles can freely diffuse to the extent permitted by ξ. The colloidal particles in region II need to hop from one trapping site to another of size ξ to diffuse longer distances. At the lowest frequencies of region I, almost all particles are trapped within the size domain L and this decreases mobility to negligible levels.

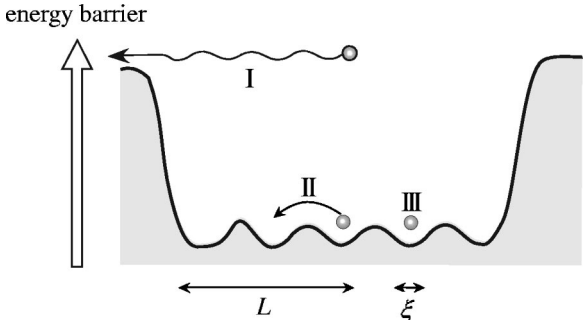

FIG. 6. Schematic representation of the mechanism of the relaxations observed in the frequency spectrum of $\mu^*(\omega)$.

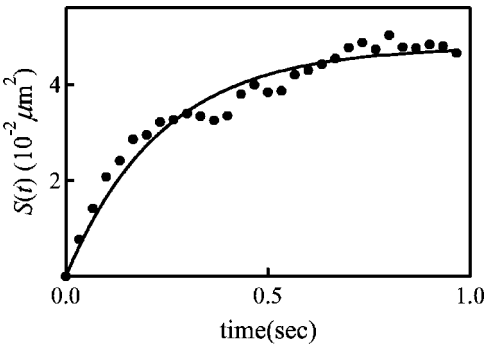

FIG. 7. Time evolution of the mean-squared displacement of a colloidal particle dispersed in a lamellar phase of $\phi_m = 5.9\%$. The solid line is a best-fit curve derived from Eq. (7).

B. Particle tracking fluorescent microscopy

As mentioned in the preceding section, LF relaxation is caused by the potential barrier of the size of the persistent length. However, it is intuitively difficult to understand why the colloidal particles are so strongly trapped within the persistent length. The influence of persistence length on the mobility of latex particles is perhaps screened by lamellar ordering. The main motivation to measure the position of a colloidal particle $\mathbf{r}_c(t)$ directly with fluorescent microscopy isto confirm whether the colloidal particle is really trapped within L. Since the upper limit of time resolution of measurement is determined by video frequency (30 Hz), it is possible to observe LF relaxation with the use of this technique. Furthermore, direct observation under a microscope allows us to confirm that the dispersed colloids do not aggregate and that they are dispersed homogenously in the lamellar matrix.

One typical example of the mean square displacement $S(t) = \langle [\mathbf{r}_c(t_0+t) - \mathbf{r}_c(t_0)]^2 \rangle_{t_0}$ of a colloidal particle dispersed in the sample of $\phi_m = 5.9\%$ is shown in Fig. 7. If we observe colloidal particles dispersed in a purely viscous matrix, time evolution of square displacement $S(t)$ should be proportional to elapsed time t. However, in the case of a lamellar solution, $\sqrt{S(t)}$ saturates to a value approximating $\sim$300 nm. This roughly coincides with Λ_L estimated from the LF relaxation of $\mu^*(\omega)$. This indicates that particles are really trapped within the space of Λ_L and that mobility is almost reduced to zero in region I. The mean square displacement of probe particles rigidly trapped in the potential barrier is given as

$$S(t) = 2\langle \mathbf{r}_2^c \rangle [1 - \exp(-t/\tau_c)]. \tag{7}$$

The characteristic relaxation frequency obtained from the particle tracking method $(1/2\pi\tau_c)$ is 0.6 Hz, and is also of the same order as the relaxation frequency of LF relaxation f_L of $\mu^*(\omega)$.

In Figs. 8 and 5(b), the dependence of τ_c and $\sqrt{\langle \mathbf{r}_2^c \rangle}$ on ϕ_m is shown together with τ_L and Λ_L obtained from $\mu^*(\omega)$. The relaxation time obtained from fluorescent microscopy is always approximately two to three times larger than that obtained from $\mu^*(\omega)$. This is probably not only a result of differences in particle size, but also of the increase in drag coefficient due to the wall effect. On the other hand, the length of fluctuation estimated from $\mu^*(\omega)$ is larger than that

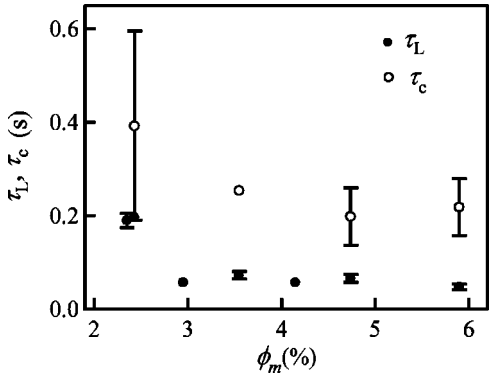

FIG. 8. Comparison of relaxation time of LF relaxation τ_L observed in complex electrophoretic mobility (filled circles) and τ_c measured by the tracking of the particle by fluorescent microscopy (open circles).

obtained from fluorescent microscopy. For a slower relaxation, colloidal particles do not freely fluctuate within Λ_L. Particles should move parallel to the membrane. In such a case, Λ_L represents the total path length within the trapping potential, which must always be longer than $\sqrt{\langle \mathbf{r}_2^c \rangle}$.

C. Dielectric spectroscopy

It is necessary to know the electrical property of a sample in order to discuss the detailed mechanism of the observed relaxations. We therefore measured the dielectric response of the sample solution. The typical frequency spectrum of permittivity $\varepsilon(\omega)$ and conductivity $\sigma(\omega)$ obtained for a sample of ϕ=3.6% is shown in Fig. 9. The spectrum reveals two relaxation processes at approximately 1 kHz and 100 kHz, which are, respectively, numbered 1 and 2 for convenience. The solid lines in Fig. 9 are best-fit curves of the sum of two Cole-Cole type relaxation spectra given by

$$\varepsilon^*(\omega) = \varepsilon_\infty + \sum_{i=1,2} \frac{\Delta\varepsilon_i}{1 + (i\omega\tau_i)^{\beta_i}} + \frac{\sigma}{i\omega} + \frac{\delta}{(i\omega)^\gamma}, \tag{8}$$

where ε_∞ is the permittivity at high frequencies, $\Delta\varepsilon_i$, τ_i and $\beta_i (i=1,2)$ are, respectively, the dielectric increment, relaxation time and broadness factor of relaxation time, and σ_{dc} is the DC conductivity. The last term of Eq. (8) represents the electrode polarization at low frequencies, and is very large in an aqueous conductive solution.

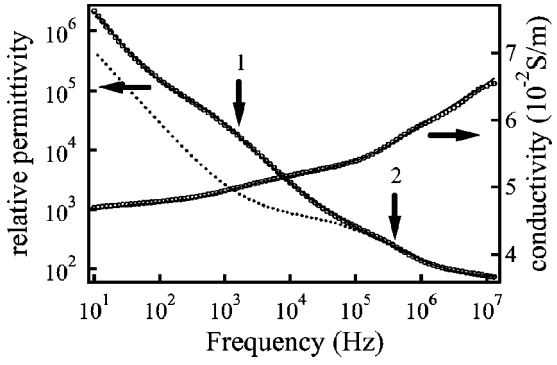

FIG. 9. Frequency dependence of permittivity and conductivity of a lamellar phase of ϕ_m=3.6% including colloidal particles (open circles). The solid lines are best-fit curves derived from Eq. (8). Dotted line is permittivity of the same sample without colloidal particles.

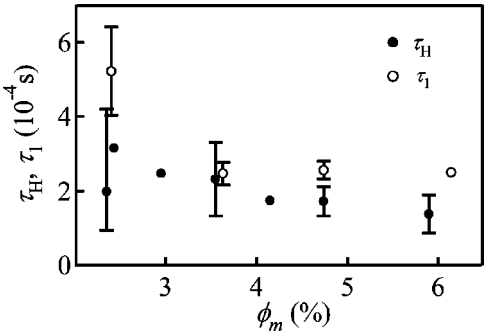

FIG. 10. Concentration ϕ_m dependence of HF relaxation time τ_H of complex electrophoretic mobility (filled circles) and relaxation time for process 1 τ_1 observed in dielectric response (open circles).

Relaxation 1 is observed only when the probe particles are added to a lamellar solution, and its relaxation time is almost the same as that of HF relaxation observed in $\mu^*(\omega)$ as shown in Fig. 10. This indicates that induced dipole moment arises at this frequency due to the constraints of in-plane motion of charged particles within ξ. The dielectric increment $\Delta\varepsilon_1$ and the relaxation time τ_1 of induced polarization due to charged colloids trapped within a potential of a size ξ are, respectively, written as

$$\Delta\varepsilon_1 \sim \frac{n_c Q^2 (\mu_{III} - \mu_{II}) \xi^2}{2k_B T \mu_{III}} \tag{9a}$$

and

$$\tau_1 \sim \xi^2 / 2D_{III}, \tag{9b}$$

where n_c and Q are the number density and charge of colloidal particles, and D_{III} is the diffusion coefficient in region III. In fact, $\Delta\varepsilon_1 \phi_m^2$ is linearly dependent on n_c as shown in Fig. 11, due to the simple relation $\xi \sim 1/\phi$. The slope of the best-fit line shown as a solid line in Fig. 11 gives $(\mu_{III} - \mu_{II}) Q^2 / 2k_B T \mu_{III} \sim 2.9 \times 10^{-12}$ C^2/Nm^2. Employing the ap-

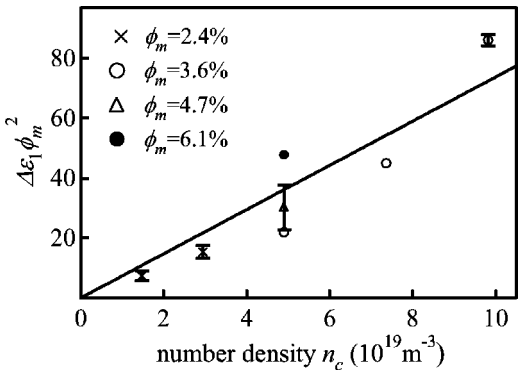

FIG. 11. Dependence of $\Delta\varepsilon_1 \phi_m^2$ on the number density of colloidal particles n_c. Surfactant concentration ϕ_m of each point is identified by different symbols. Solid line is a best-fit line assuming a linear relation.

proximate value of $(\mu_{III}-\mu_{II})/\mu_{III}\sim 0.3$, the surface charge per colloidal particle is represented by $Q\sim 2.8\times 10^{-16}$ C, which coincides with the value measured by titration 2.4×10^{-16} C. It is shown that the mechanism of relaxation 1 of the dielectric response is the same as that of HF relaxation of complex electrophoretic mobility.

On the other hand, a faster relaxation process (relaxation 2) is always observed even without the presence of colloidal particles in the sample solution. We have recently shown [12] that the dielectric response of a lyotropic lamellar phase can be modeled as a series circuit of capacitance (membranes) and resistance (solvent), which causes a so-called Maxwell-Wagner relaxation in dielectric response. At frequencies lower than those of a Maxwell-Wagner relaxation, a component of the electric field vertical to the membrane is applied mainly to the capacitance (membrane), and the electric field in the aqueous phase is forced to lie parallel to the membranes. This implies that HF relaxation in $\mu^*(\omega)$ is caused by the hindrance of Brownian motion of colloidal particles parallel to membranes, since the frequency range in which $\mu^*(\omega)$ was measured is always below the Maxwell-Wagner relaxation frequency.

V. DISCUSSION

A. Effective friction coefficient in the lamellar phase

If colloidal particles can freely diffuse to an extent permitted by ξ and at a frequency within region III, the drag coefficient γ_{III} is estimated from the observed mobility μ_{III} by Eq. (5). Open circles in Fig. 12 show the $1/\xi$ dependence of the ratio of $\gamma_0(\equiv 6\pi\eta_0 a)$to γ_{III} calculated from μ_{III}.

At the lowest frequency in region III, HF relaxation arises due to the trapping potential of size Λ_H. Since its relaxation time τ_H is written as $\tau_H\sim\Lambda_H^2/2D_{III}=\gamma_{III}\Lambda_H^2/2k_BT$, γ_{III} can also be estimated from τ_H as

$$\gamma_{III}=2k_BT\tau_H/\xi^2 \tag{10}$$

by assuming $\Lambda_H\sim\xi$. The values of γ_0/γ_{III} calculated by this method are plotted as closed circles in Fig. 12 and are in approximate agreement with values obtained from mobility without any assumptions.

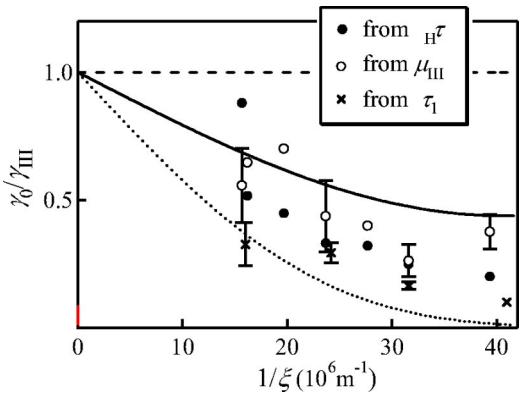

FIG. 12. Half of the interlamellar space $\xi(=d/2)$ dependence of the ratio of drag coefficient γ_0/γ_{III} calculated from μ_{III} (open circles), from relaxation time τ_H (closed circles) and from τ_1 (crosses). The length ξ is calculated from the volume fraction ϕ_m using the simple swelling law. The solid curve and dotted curve are theoretically calculated values for a spherical particle between parallel walls (separation 2ξ) and in a cylindrical wall (radius ξ), respectively.

The estimated value of γ_{III} is always larger than γ_0 and increases with ϕ_m. That is not due to the existence of certain relaxations at frequencies higher than those found in region III, but is due to the excess stress caused by the confinement of particles between membrane walls. The drag coefficient for a spherical particle near a hard boundary wall under no-slip conditions has been calculated as [24]

$$\frac{\gamma_0}{\gamma}=1-1.004\left(\frac{a}{\xi}\right)+0.418\left(\frac{a}{\xi}\right)^3+0.21\left(\frac{a}{\xi}\right)^4-0.169\left(\frac{a}{\xi}\right)^5 \tag{11}$$

for infinite parallel plates separated by a distance 2ξ (solid curve in Fig. 12), and as

$$\frac{\gamma_0}{\gamma}=\frac{1-2.1050(a/\xi)+2.0865(a/\xi)^3-1.7068(a/\xi)^5+0.726\ 03(a/\xi)^6}{1-0.758\ 57(a/\xi)^5} \tag{12}$$

for an infinite cylinder with radius ξ (dotted curve in Fig. 12). The excess stress experienced by a moving particle can be roughly explained by the geometry of the wall surrounding the particle. There is two-dimensional free space for a probe particle in a slit between parallel flat plates, but there is only one dimension of free space in a cylinder. If the bilayer membrane is not regarded as a flat wall, and it is believed that a colliding point of membranes also disturbs the flow field, it is reasonable to expect that experimental data lie between these theoretical curves.

The potential contribution of other factors should be taken into consideration.

(1) Equations (11) and (12) are calculated only for particle movement that is restricted to the centerline of each wall, while it is experimentally known that the position dependence of γ_0/γ_{III} is not that large, except for particles attachedto the wall [25].

(2) The strength and direction of the electric field that is applied to colloidal particles is somewhat heterogeneous.

(3) It is generally accepted that the no-slip boundary con-

dition is not satisfied when considering the interface of bilayer membranes.

However, these weaker effects may counteract each other and would only require a negligible correction to data. Therefore, the result shown in Fig. 12 suggests that the drag coefficient in a nanometer-sized structure can be roughly estimated by continuum hydrodynamics, and that there is no relaxation process at frequencies higher than the measured frequency range.

B. Mechanism of HF relaxation

1. Dynamic disorder transport

Dielectric spectroscopy indicates that the HF mode is not caused by the hindrance induced by the Brownian motion of colloidal particles vertical to membranes, but by the motion of colloidal particles parallel to membranes. It is therefore tentatively assumed that colloidal particles are weakly confined within the length between the colliding points of membranes, neglecting the discrepancy of length scale ($\Lambda_{\mathrm{H}} \sim d/2$ and $l=4d\sim 7d$). At middle frequencies (region II), colloidal particles need to hop between trapping sites to diffuse longer distances, while colloidal particles may diffuse without hopping if membrane collision disappears with time. Such a process is called dynamic disorder transport [14]. When this transport process is taken into account, the theoretical spectrum of mobility $\mu^*(\omega)$ can be rewritten as

$$\mu^*(\omega) = \mu_0 + \Delta\mu \frac{\tau_f(1+i\omega\tau_m)}{\tau_f+\tau_m+i\omega\tau_f\tau_m}, \tag{13}$$

where $\tau_m \sim \eta\xi^3/k_c$ is the reorganization time of a trapping site, which is the relaxation time of fluctuation for a free membrane of size ξ [26], $\tau_f \sim \eta a\xi^2/k_BT$ is the time required for probe particles to diffuse over ξ, and $\Delta\mu$ is the increment of mobility under the condition involving the absence of a dynamic disorder process. From Eq. (13), $\mu_{\mathrm{II}}/\mu_{\mathrm{III}}$ is roughly written as

$$\frac{\mu_{\mathrm{II}}}{\mu_{\mathrm{III}}} = \frac{\mu_0 + \Delta\mu(\tau_f/(\tau_f+\tau_m))}{\mu_0+\Delta\mu}, \tag{14}$$

which is a monotonously increasing function of membrane concentration ϕ_m. However, experimental values of $\mu_{\mathrm{II}}/\mu_{\mathrm{III}}$ represent a decreasing function of ϕ_m, as shown in Fig. 13. This discrepancy indicates that generation and annihilation of colliding points of membranes have little influence on the diffusion of colloidal particles, which is plausible because colloidal particles can easily bypass the colliding points.

2. Distortion field induced by dispersed particles

In the above discussions, it is not assumed that the local morphology of membranes is influenced by colloidal particles. However, the membranes in this study are so soft that they are easily deformed by the osmotic pressure produced by the collision of colloidal particles with the membranes. This distortion field surrounds a colloidal particle and is essential for the understanding of HF relaxation. As shown in Fig. 14, the distortion field is described by the displacement

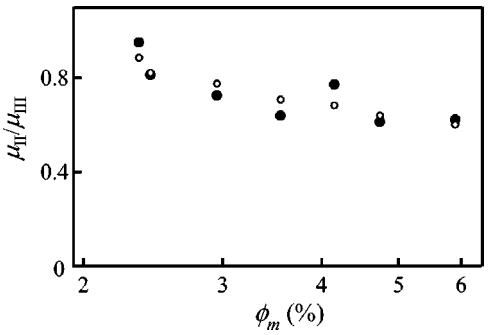

FIG. 13. Concentration dependence of the ratio of the complex electrophoretic mobility, $\mu_{\mathrm{II}}/\mu_{\mathrm{III}}$ (filled circles) and best-fit values as derived from Eq. (37) (open circles).

of a membrane from the reference plane, which is the average membrane position in the absence of a particle, $u(\mathbf{r},z)$, where the z axis is taken vertical to the membrane and the $\mathbf{r}$ plane is parallel to the membrane. A colloidal particle is located at the origin. The elastic energy of a smectic liquid crystal is expressed by the Landau–de Gennes Hamiltonian [27]

$$H_0 = \int d\mathbf{r} \int dz \left[\frac{1}{2}B\left(\frac{\partial u}{\partial z}\right)^2 + \frac{1}{2}K(\nabla_r^2 u)^2 \right], \tag{15}$$

where B is the layer compression modulus and K is the bending modulus of the smectic liquid crystal. By minimizing this Landau-de Gennes Hamiltonian under the constraint for local spacing, $d_\pi = d + \Delta d_0$, Sens *et al.* calculated the distortion field $u(\mathbf{r},z)$ [13] as

$$u(\mathbf{r},z) = \frac{d\Delta d_0}{4z}\exp\left(\frac{-r^2}{4\lambda|z|}\right), \tag{16}$$

where $\lambda \equiv \sqrt{K/B}$ is represented by d since B and K are roughly estimated as $B\sim(k_BT)^2/k_cd^3$ and $K\sim k_c/d$, respectively, in the case of lyotropic smectics. The distortion of a neighboring membrane is therefore given as

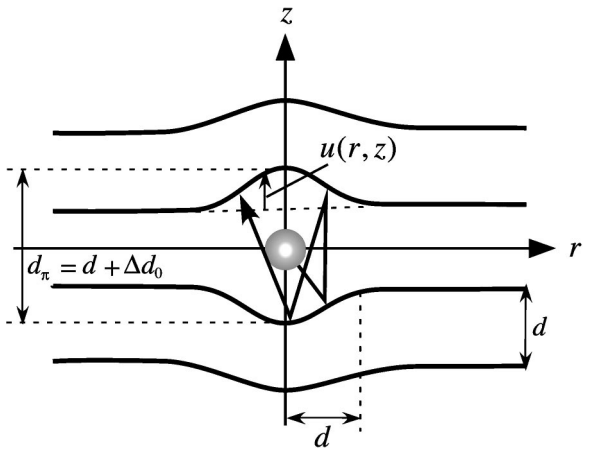

FIG. 14. Schematic drawing of membranes distorted by the collision with colloidal particles.

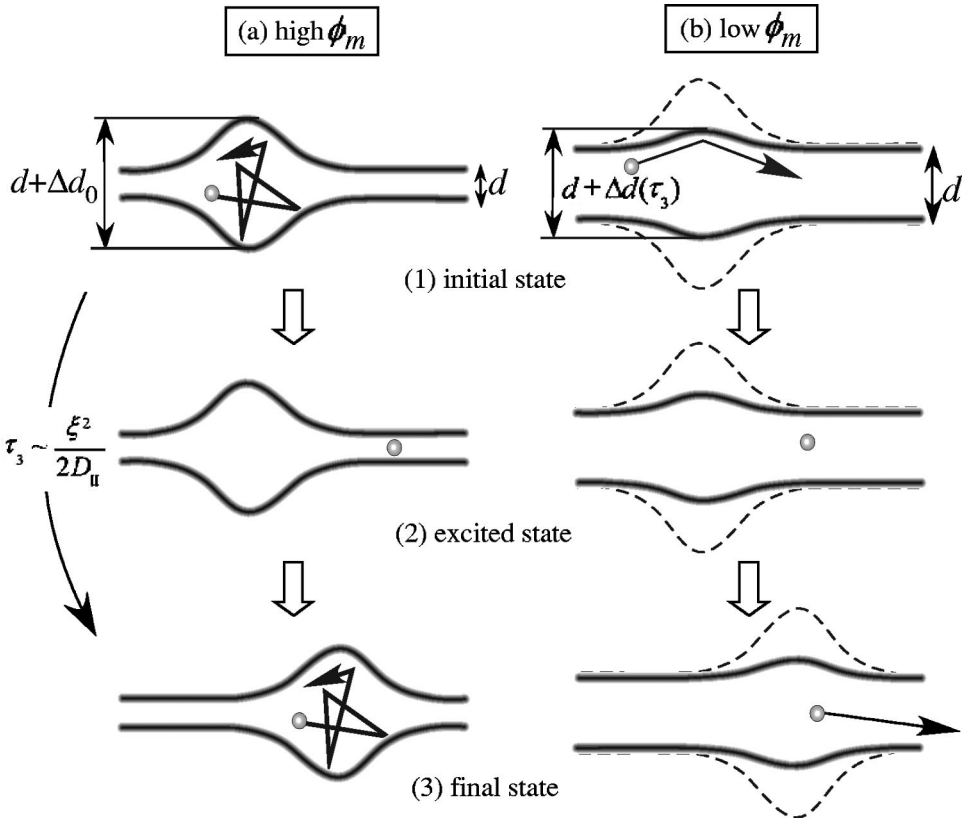

FIG. 15. Diffusion process of colloidal particles between soft membranes. A colloidal particle fluctuates in a distortion field (1, initial state) hops out (2, excited state), then creates a distortion field around itself (3, final state). At (a) high ϕ_m, a strongly interacted particle-distortion pair always grows fully while at (b) low ϕ_m, the colloidal particle moves too fast to form a substantial distortion field.

$$u(\mathbf{r},d/2)=\frac{\Delta d_0}{2}\exp\left(\frac{-r^2}{2d^2}\right). \tag{17}$$

It is important that the in-plane size of distortion of a neighboring membrane is roughly estimated as d. This indicates that the in-plane motion of a colloidal particle is free within d while a colloidal particle has to drag the distortion field to move a distance longer than d. This is the probable origin of HF relaxation.

A sequence representing the Brownian motion of colloidal particles influenced by the distortion field is illustrated in Fig. 15. A colloidal particle fluctuating in the distortion field hops out, and then creates a distortion field around itself. In the excited state [(2) in Fig. 15], the space available for the colloidal particle ($\sim d$) is smaller than that in the initial state ($\sim d+\Delta d_0$). This entropy loss gives rise to the energy barrier ΔU for this hopping process, which is written as

$$k_BT\ln(1+\Delta d_0/d). \tag{18}$$

Therefore, the ratio of μ_{II} to μ_{III} is expressed by the amplitude of the distortion field as

$$\frac{\mu_{\mathrm{II}}}{\mu_{\mathrm{III}}}\sim\frac{d}{d+\Delta d_0}. \tag{19}$$

The total free-energy F of this particle-distortion pair is the sum of the elastic energy of the distortion field and the entropy of a colloidal particle. Since the elastic energy of the distortion field is estimated by incorporating Eq. (16) into (15) as $k_BT(\Delta d_0/d)^2$ [13], it is written as

$$F\sim k_BT[(\Delta d_0/d)^2-\ln(1+\Delta d_0/d)]. \tag{20}$$

By minimizing F with Δd_0, the amplitude of distortion Δd_0 is given as

$$\Delta d_0=\frac{\sqrt{3}-1}{2}d_0\sim 0.4d. \tag{21}$$

Since the measured value of $\mu_{\mathrm{II}}/\mu_{\mathrm{III}}$ averaged over all concentrations is about $2/3$, a membrane can theoretically distort to a sufficient degree to yield the observed HF relaxation.

3. Step response of the distortion field

We have so far neglected the dynamic process concerning the formation of the distortion field. This is very important because a distortion field cannot grow sufficiently if a colloidal particle escapes from the field too quickly. In order to evaluate such a dynamic effect, we discuss the step response function of the distortion field $u(\mathbf{r},z,t)$ by calculating the hydrodynamic equation of a lyotropic lamellar phase. A basic set of hydrodynamic equations for a lyotropic lamellar phase is presented in Appendix B. When osmotic pressure Π due to a colloidal particle dispersed between membranes is introduced as

$$\Pi=\Pi_0\delta(\mathbf{r},z), \tag{22}$$

Eq. (B4) is modified because of the stress applied to membranes

$$\rho\frac{\partial v_z}{\partial t} = -\frac{\partial p}{\partial z} + \frac{\partial}{\partial z}\left[\frac{\partial f_1}{\partial \tilde{\gamma}}\right]_{\tilde{\gamma}} - K\left(\frac{\partial^4 u}{\partial x^4} + 2\frac{\partial^4 u}{\partial x^2\,\partial y^2} + \frac{\partial^4 u}{\partial y^4}\right) + \eta\left[\frac{\partial^2}{\partial x^2} + \frac{\partial^2}{\partial y^2} + \frac{\partial^2}{\partial z^2}\right]v_z - \frac{\partial \Pi}{\partial z}. \tag{23}$$

The derivation of deformation is performed in the Fourier space. In order to consider the purely diffusive slow mode, inertial terms in hydrodynamic equations are neglected. From Eqs. (23), (B2), (B3), (B5), and (B6), we obtain

$$q^4\eta\frac{\partial^2}{\partial t^2}u_q + q_r^2[\mu_s\eta q^4 D_{33} + Kq_r^4 + (B - 2D_{23} + D_{33})q_z^2]\frac{\partial}{\partial t}u_q + \mu_s q_r^4[(D_{33}q_r^4K - D_{23}^2q_z^2 + BD_{33}q_z^2)u_q + iD_{33}q_z\Pi_q] = 0, \tag{24}$$

where $A_q(u_q,\Pi_q)$ is the Fourier component of quantity A defined as

$$A(\mathbf{r},z) = \frac{1}{(2\pi)^3}\int\int d\mathbf{q}_r\, dq_z\, A_q \exp[i(\mathbf{q}_r\cdot\mathbf{r} + q_z z)], \tag{25}$$

and $\mathbf{q}_r$ and q_z are the Fourier conjugates of $\mathbf{r}$ and z, respectively. A stationary solution for u_q is given as

$$u_{q0} = -\frac{iD_{33}q_z\Pi_q}{D_{33}q_r^4K - D_{23}^2q_z^2 + BD_{33}q_z^2} \sim -\frac{iq_z\Pi_q}{Kq_r^4 + Bq_z^2}. \tag{26}$$

Since the energy cost for changing the area per surfactant molecule is usually much larger than the other deformation modes, the plausible relation $D_{33} \gg B, D_{23}$ is assumed. In this case, the same solution as represented by Eq. (16) is obtained by the inverse transform of Eq. (26). At equilibrium, the amplitude of distortion as determined by the osmotic pressure is given as $\Delta d_0 = \Pi_0/2\pi d\sqrt{BK}$.

The higher derivative term of t in Eq. (24) usually corresponds to the membrane peristaltic and second sound modes. Schematic drawings of these hydrodynamic modes are given in Figs. 6.8(b) and 6.8(d) in Ref. [10], respectively, and are probably not comparable to the slower modes of current interest. When we neglect terms including the second derivative of t, an equation representing the so-called undulation-baroclinic mode [see Figs. 6.8(a) and 6.8(c) in Ref. [10]) is obtained

$$[\mu_s\eta q^4 D_{33} + Kq_r^4 + (B - 2D_{23} + D_{33})q_z^2]\frac{\partial}{\partial t}u_q = -\mu_s q_r^2[(D_{33}q_r^4K - D_{23}^2q_z^2 + BD_{33}q_z^2)u_q + iD_{33}q_z\Pi_q]. \tag{27}$$

The solution of this equation is given as

$$u_q(t) = u_{q0}[1 - \exp(-\Gamma t)], \tag{28}$$

where

$$\Gamma = \frac{\mu_s D_{33}(Kq_r^4 + Bq_z^2)q_r^2}{Kq_r^4 + \mu_s\eta D_{33}q^4 + D_{33}q_z^2}. \tag{29}$$

Therefore, the inverse Fourier transformation of u_q written as a superposition of undulation-baroclinic modes gives the step response of distortion of membranes,

$$u(\mathbf{r},z,t) = \frac{1}{(2\pi)^3}\int\int d\mathbf{q}_r\, dq_z \frac{-iq_z\Pi_q}{Kq_r^4 + Bq_z^2}[1 - \exp(-\Gamma t)]\exp[i(\mathbf{q}_r\cdot\mathbf{r} + q_z z)]. \tag{30}$$

Instead of calculating an analytical form of this solution by finding all residues, here we make plausible approximations. First, Kq_r^4 in the denominator of Eq. (29) is much smaller than the other two terms, except for the case of $q_z \sim 0$. Since u_{q0} has a negligible value in the case of $q_z \sim 0$, it is always possible to ignore the term (Kq_r^4) in Eq. (29). Second, Γ is a monotonically decreasing function of q_z which asymptotically approaches $\Gamma \sim k_B T q_r^2/12\eta d$ at $q_z \gg q_r$ from the maximum value of $\Gamma \sim k_B T q_r^2/\eta d$ at $q_z \ll q_r$. The prefactor $-iq_z\Pi_q/(Kq_r^4 + Bq_z^2)$ in Eq. (30) has a maximum value in the intermediate region of these two extremes at $q_z = \sqrt{K/B}q_r^2$. We can therefore fix Γ to the value $\Gamma(q_z = \sqrt{K/B}q_r^2) = k_B T q_r^2/6\eta d \equiv \alpha q_r^2$ with little error in the estimation of $u(\mathbf{r},z,t)$. Now, Eq. (30) can be integrated over q_z and rewritten as

$$u(\mathbf{r},z,t) = \frac{\Delta d_0 d\lambda}{4\pi}\int d\mathbf{q}_r[1 - \exp(-\alpha q_r^2 t)]\exp(-\lambda q_r^2 z)\exp[i(\mathbf{q}_r\cdot\mathbf{r})]. \tag{31}$$

The time-dependent component of Eq. (31) is obtained simply by replacing the variable z in Eq. (15) with $z + \alpha t/\lambda$, and an approximated form of $u(\mathbf{r},z,t)$ is given by

$$u(\mathbf{r},z,t) = \frac{\Delta d_0 d}{4z}\exp\left(-\frac{r^2}{4\lambda z}\right) - \frac{\lambda \Delta d_0 d}{4(\lambda z+\alpha t)}\exp\left[-\frac{r^2}{4(\lambda z+\alpha t)}\right]. \tag{32}$$

The step response for the increment of lamellar spacing $\Delta d(t) \equiv 2u(0,d/2,t)$ is obtained from this equation as

$$\Delta d(t) = \Delta d_0\left(\frac{k_B T t}{3\eta d^3 + k_B T t}\right). \tag{33}$$

The characteristic time τ_R for the formation of a distortion field is therefore estimated as

$$\tau_R \sim \frac{3\eta d^3}{k_B T}. \tag{34}$$

4. Effect of dynamics of distortion field formation

Now we can consider the influence of the dynamic process of the formation of a distortion field on the transport property of colloidal particles. Since a distortion field grows only when the colloidal particle stays inside, the amplitude of the distortion field is estimated as $\Delta d(\tau_3)$, where τ_3 is the average time for one hopping event estimated as $\tau_3 = \xi^2/2D_{\mathrm{II}}$. Therefore, this hopping time τ_3 is proportional to ϕ_m^{-2}. On the other hand, the time required for the formation of a distortion field τ_R is proportional to ϕ_m^{-3}. Therefore, as shown in Fig. 15, at a high concentration where τ_3 is larger than τ_R, the distortion field can grow completely around a colloidal particle. On the other hand, at low concentrations where τ_3 is smaller than τ_R, the distortion field cannot grow sufficiently.

In the same manner as discussed in Sec. V B 2, $\mu_{\mathrm{II}}/\mu_{\mathrm{III}}$ is given by the ratio of the amplitude of the distortion field as

$$\frac{\mu_{\mathrm{II}}}{\mu_{\mathrm{III}}} = \frac{d}{d+\Delta d(\tau_3)}. \tag{35}$$

From the relations of $\tau_3 = \xi^2/2D_{\mathrm{II}}$ and $\tau_{\mathrm{H}} = \xi^2/2D_{\mathrm{III}}$, τ_3 is estimated by the measured parameters τ_{H}, μ_{III}, and μ_{II} as

$$\tau_3 = \tau_{\mathrm{H}}\frac{D_{\mathrm{III}}}{D_{\mathrm{II}}} = \tau_{\mathrm{H}}\frac{\mu_{\mathrm{III}}}{\mu_{\mathrm{II}}}. \tag{36}$$

From Eqs. (33), (35), and (36), the dependence of $\mu_{\mathrm{II}}/\mu_{\mathrm{III}}$ on ϕ_m is given as

$$\frac{\mu_{\mathrm{II}}}{\mu_{\mathrm{III}}} = \frac{3\eta d^4 - (d+\Delta d_0)k_B T\tau_{\mathrm{H}} + \sqrt{12\eta k_B T\tau_{\mathrm{H}} d^5 + [(d+\Delta d_0)k_B T\tau_{\mathrm{H}} - 3\eta d^4]^2}}{6\eta d^4}. \tag{37}$$

In Fig. 13, experimental values of $\mu_{\mathrm{II}}/\mu_{\mathrm{III}}$ are plotted and shown as filled circles. Empty circles are best-fit values with respect to Eq. (37). Since τ_{H} is obtained experimentally for each concentration, a continuous line could not be obtained in this case. It is noted that only one fitting parameter $\Delta d_0 = 0.9d$ determines the level of $\mu_{\mathrm{II}}/\mu_{\mathrm{III}}$ at a high concentration limit. The crossover concentration to a lower concentration limit is automatically given by Eq. (37), regardless of the fitting parameter Δd_0. It is therefore confirmed that the distortion field created by colloidal particles constrains the in-plane motion of a colloidal particle, and this phenomenon corresponds to the mechanism of HF relaxation.

C. Mechanism of LF relaxation

Since the lamellar in our sample cell is not macroscopically oriented, there must be defects in a scale larger than the intermembrane distance. In fact, a vesicle-like structure or a folded lamellar surrounded by a perforated lamellar is frequently observed in freeze fracture electron micrographs [28,29]. We have recently measured the dielectric response in the lyotropic lamellar phase of an aqueous solution of $C_{12}E_5$, and reported [12] that the observed Maxwell-Wagner relaxation can be quantitatively understood by modeling the lamellar phase as aggregates of multilamellar vesicles, the insides and outsides of which are filled with perforated lamellar. The size of such vesiclelike regions estimated from dielectric spectroscopy is approximately 200–400 nm, which coincides with Λ_{L} obtained in this study. It is plausible that the trapping sites for LF relaxation are composed of multilamellar vesicles which colloidal particles cannot move across. On the other hand, colloidal particles can move inside and outside of the vesiclelike region, which is composed of perforated lamellar.

Therefore, the Brownian motion of colloidal particles in region I should be closely related to the property or dynamics of a site-connecting path, which probably consists of microscopic defects joining one bilayer to another. We do not assume that colloidal particles can hop between different sites by breaking through the membranes of vesiclelike structures, since an extremely large amount of energy would be required for such a move [30]. There are therefore two possible mechanisms to effect the movement of colloidal particles through the path: (1) colloidal particles may search for a very small fraction of the stable path, and (2) the dy-

namic reorganization of lamellar structure may lead to the very slow diffusion of colloidal particles. The latter case would involve a mechanism of LF relaxation equivalent to dynamic disorder transport [14].

Figure 16(a) shows a typical trajectory of a colloidal particle dispersed in the lamellar phase of $\phi_m=2.4\%$ as observed by fluorescent microscopy. The colloidal particle hops many times between particular sites through a path fixed for some time [site A and B in Fig. 16(a)]. Figure 16(c) shows the average number of sites connecting the observed path. The number seems to be a decreasing function of ϕ_m. In fact, almost all colloidal particles dispersed in concentrated solutions are always trapped in one particular site, as shown in the typical trajectory of $\phi_m=4.7\%$ [Fig. 16(b)]. The occurrence of sites associated with a path is rare in concentrated solutions since more microscopic defects are required fora single path. This is consistent with the fact that the effective size of the potential barrier Λ_L becomes large when ϕ_m decreases, as shown in Fig. 5(b). It is noted, however, that the intrinsic size of the trapping site has little dependence on concentration of the surfactant, as shown in Figs. 16(a) and 16(b) since the size of the vesiclelike region is mainly determined by the nature of a single membrane [12].

On the other hand, a colloidal particle trapped within particular sites [A and B in Fig. 16(a)] hops to another site (C), which was probably induced by the reorganization of the lamellar structure. It is rare to observe such an event that implies a renewal of the site-connecting path during the period of each experimental (20 s). Therefore, it is difficult to obtain the renewal rate p from this measurement. However, this observation suggests that the diffusion process in region I mainly follows a mechanism reflective of dynamic disorder transport.

It is expected that μ_I/μ_{II} gives important information on the renewal rate p of the site-connecting path. However, μ_I is not obtained from the frequency spectrum of $\mu^*(\omega)$ since mobility relaxes to a negligible value in region I. μ_I can probably be determined from the self-diffusion coefficient of probe particles in this region, D_I. In order to obtain D_I, the diffusion of probe particles has to be tracked for a distance that is much longer than L, and would involve a tracking period exceeding hundreds of seconds. This is experimentally difficult because colloidal particles move out of the focal plane and adjusting the z-stage position results in large drifting motions of colloidal particles. In this study, D_I in a sample of $\phi_m=4.7\%$ was measured by slight modification of our experimental system [8,9] for the mobility as explained in Appendix A. Since we set the scattering angle to satisfy the condition $2\pi/q\approx 3\ \mu\mathrm{m}>L$, the probe particles need to diffuse about 3 μm by hopping between trapping sites of size L before the intensity of the scattered light $[\propto A_1''(t)]$ loses its memory, and we can regard the value of the apparent diffusion constant as D_I. The autocorrelation function of the amplitude of the fundamental signal $g(t)=\langle A_1''(t)A_1''(0)\rangle \propto \exp(-D_I q^2 t)$ obtained for the sample of $\phi_m=4.7\%$ is shown in Fig. 17. A very slow fluctuation with correlation time $1/D_I q^2\approx 230$ s is observed. The estimated value of γ_I is much larger (about 1.4×10^4 times) than that of γ_0. Such extremely large values of γ_I again indicate that the probe particles are almost completely trapped within L of region I. From an approximate length between trapping sites of 1 μm, the renewal rate p is estimated as $p\sim D_I/L^2\sim 3\times10^{-3}\ \mathrm{s}^{-1}$. We consider this a maximum estimation of p since it is dif-

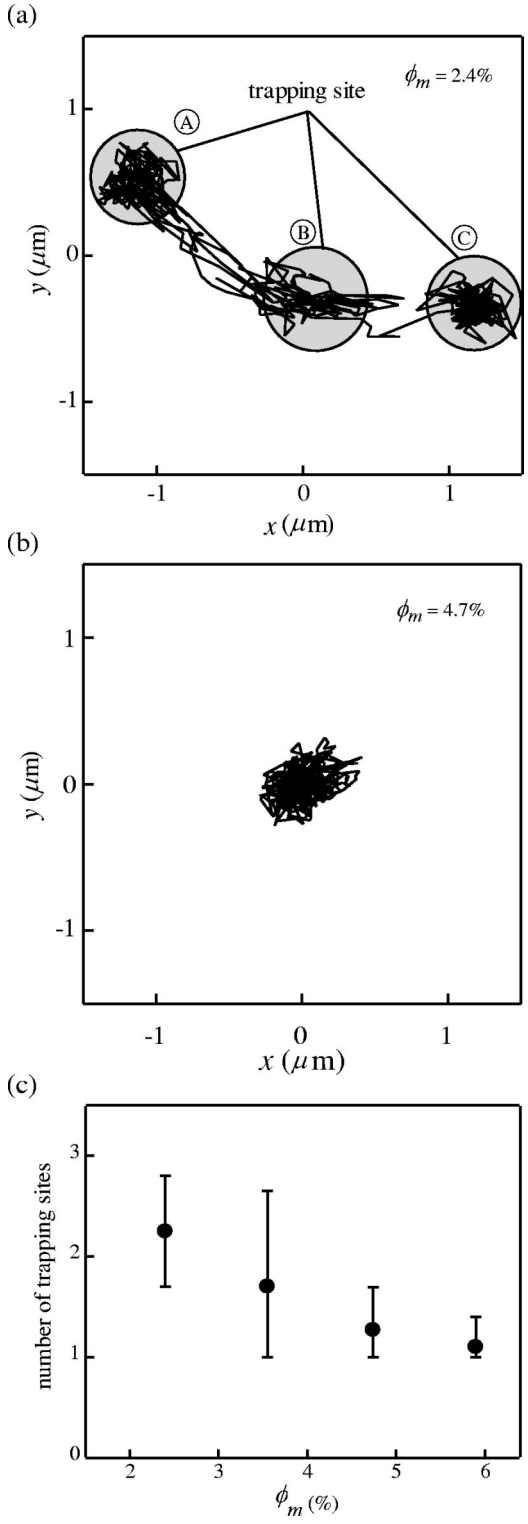

FIG. 16. Typical trajectories of a colloidal particle dispersed in lamellar phase over 20 s for (a) $\phi_m=2.4\%$ and (b) $\phi_m=4.7\%$, and (c) concentration dependence of the average number of trapping sites observed during 20 s.

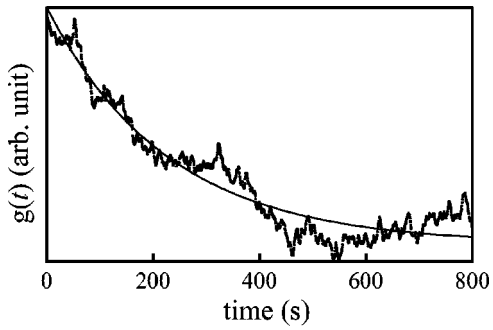

FIG. 17. Autocorrelation function of the amplitude of the fundamental component $\langle A_1''(t)A_1''(0)\rangle$ in a lamellar phase ($\phi_m = 4.7\%$). The solid line is a best-fit curve of exponentially decaying function.

ficult to distinguish between the diffusion of a colloidal particle and drift. We are therefore now measuring p by a more direct method. This is possible if we make an artificial path by manipulating an optically trapped colloidal particle, and then observe the relaxation of the path by measuring the yield stress. Recent results show consistent value of p with that obtained in this study [33].

VI. CONCLUDING REMARKS

In conclusion, we studied the spectra of complex electrophoretic mobility $\mu^*(\omega)$ of nanometer-sized colloidal particles dispersed in a nonionic dilute lamellar phase in order to probe the rheological properties in microscopic scales. The spectra show two relaxations corresponding to the two characteristic lengths of the lamellar structure. Combining the complementary information given by dielectric spectroscopy and the tracking of a particle's motion with fluorescent microscopy, the detailed mechanism of the observed relaxations were investigated. It was found that these relaxations offer more information on the local structure and interaction between particles and membranes than information yielded by conventional macrorheology. This is because the probe particles are smaller than the characteristic length (intermembrane distance d) of the lamellar phase, and wide-band spectroscopy is possible in our experimental system. The transport properties of colloidal particles between membranes are analogous to those of proteins and other secretions in biological systems in which bilayer membranes are one of the most common components. As a consequence, the method of electrophoretic microrheology developed in this study represents a useful method for the study of transport phenomena in much more complex systems, such as biological cells and other complex systems.

ACKNOWLEDGMENTS

This work is supported by a Grant-in-Aid for Scientific Research from the Japan Society for the Promotion of Science and from Ministry of Education, Culture, Sports, Science and Technology of Japan. D.M. is also supported by a grant from the Research Fellowship of Japan Society for the Promotion of Science. The authors thank T. Nishino for his technical assistance. They also thank Professor K. Ito and Dr. H. Furusawa of the University of Tokyo for kindly giving them a chance to access their fluorescent microscope in this study.

APPENDIX A: PRINCIPLES OF WIDE-BAND SPECTROSCOPY OF $\mu^*(\omega)$

As written in the text, the wide-band spectroscopy of $\mu^*(\omega)$ is carried out with a recently developed method using the heterodyne technique of dynamic light scattering. If the suspension is composed of identical spherical particles without any internal degree of freedom, the scattered electric field $E_S(t)$ from the spheres at position $\mathbf{r}_n$ is given by $\sqrt{I/N}\Sigma_{\mathbf{n}}\exp\{i(\mathbf{q}\cdot\mathbf{r}_n - \omega_I t)\}$. Here, $I = E_S E_S^*$, N is the number of particles in the scattering volume, ω_I is the angular frequency of the incident light, and $\mathbf{q}$ is the scattering wave vector. We employ an optical heterodyne technique to obtain the electrophoretic mobility by mixing the scattered light with local light, as shown schematically in Fig. 2. The temporal change of the intensity of the detected light I_{out} is given as $E_S E_L^* + E_S^* E_L = 2\sqrt{I_0 I/N}\Sigma_n \cos(\mathbf{q}\cdot\mathbf{r}_n)$, where E_L is the electric field of the local light and $I_0 = E_L E_L^*$. In equilibrium, $\mathbf{r}_n$ varies with time due to the Brownian motion of colloidal particles. When the particles are subjected to the external electric field E, another contribution $\delta\mathbf{r}_E$ gives rise to displacement due to electrophoresis. The total displacement of a colloidal particle is given as $\mathbf{r}_n = \mathbf{r}_{0n} + \delta\mathbf{r}_{En}$, where $\mathbf{r}_{0n}$ is the position of a particle without an electric field. When the sinusoidal field $\mathbf{E} = \mathbf{E}_0 \cos(\omega t)$ is applied to suspension, $\delta\mathbf{r}_{En}$ is given by $\delta\mathbf{r}_{En} = \mu_n \mathbf{E}_0 \sin(\omega t + \delta)/\omega$. If every particle has the same mobility μ, I_{out} is given as

$$I_{\text{out}} = 2\sqrt{\frac{I_0 I}{N}}\left[\sum_n \cos(c_n)\left\{J_0(z) + 2\sum_{k=1}^{\infty} J_{2k}(z)\cos(2k(\omega t + \delta))\right\} + 2\sum_n \sin(c_n)\sum_{k=1}^{\infty} J_{2k-1}(z)\sin((2k-1)(\omega t + \delta))\right], \quad \text{(A1)}$$

where $c_n = \mathbf{q}\cdot\mathbf{r}_{0n}$, $z = \mu\mathbf{q}\cdot\mathbf{E}_0/\omega$ and J_k is the Bessel function of kth order. We hereafter call the kth order harmonic component the kth order term.

The signal detected by QELS-SEF in Eq. (A1) consists of two components. One is a randomly fluctuating component due to the Brownian motion of colloidal particles, $\Sigma_n\cos(c_n)$ and $\Sigma_n\sin(c_n)$. The diffusion coefficient D is obtained from the autocorrelation function of these parts [8]. The other component is the response to the external field, $\Sigma_{k=1}^{\infty}J_{2k}(z)\cos[2k(\omega t+\delta t)]$ and $\Sigma_{k=1}^{\infty}J_{2k-1}(z)\sin[(2k-1)(\omega t+\delta)]$. The complex electrophoretic mobility $\mu^*(\omega)$ is obtained from these parts. We therefore extract the first-order component in Eq. (A1),

$$A_1 = 4\sqrt{I_0 I/N}J_1(z)\sin(\omega t+\delta)\sum_n \sin(c_n), \tag{A2}$$

and then the second order harmonic component

$$A_2 = 4\sqrt{I_0 I/N}J_2(z)\cos(2\omega t+2\delta)\sum_n \cos(c_n) \tag{A3}$$

from the output signal. However, these components are not directly measured by a lock-in amplifier because the temporal average of $\cos(c_n)$ and $\sin(c_n)$ becomes zero.

In order to avoid this undesirable effect, we squared these signals before lock-in detection when the correlation time of $\Sigma_n\cos(c_n)$ and $\Sigma_n\sin(c_n)$ was smaller than the time constant t_c of the lock-in amplifier. Using this procedure, the components detected with the lock-in amplifier are given by

$$A_1' = -4I_0\langle I\rangle J_1^2(z)\cos(2\omega t+2\delta) \approx -I_0\langle I\rangle z^2\cos(2\omega t+2\delta) \tag{A4}$$

and

$$A_2' = 4I_0\langle I\rangle J_2^2(z)\cos(4\omega t+4\delta) \approx \tfrac{1}{16}I_0\langle I\rangle z^4\cos(4\omega t+4\delta). \tag{A5}$$

In the above calculation, we used the relation $\Sigma_{n\neq m}\cos(c_n)\cos(c_m)=0$ and $\Sigma_{n\neq m}\sin(c_n)\sin(c_m)=0$, which are derived from the plausible assumption that there are many particles having no positional correlation in a scattering volume. The phase delay of δ is obtained from Eqs. (A4) and (A5). But the magnitude μ cannot be obtained directly from the amplitude of the output signals A_1' or A_2', since they depend on uncontrollable parameters such as the fluctuation of the intensity of laser light and the efficiency of the optical system. As a result, the ratio of the amplitude A_2'/A_1' is calculated to obtain μ.

On the other hand, the correlation time of $\Sigma_n\cos(c_n)$ and $\Sigma_n\sin(c_n)$ is much larger than the time constant t_c of the lock-in amplifier used in this study. In such cases, A_1 and A_2 are detected directly with a lock-in amplifier. The output of the lock-in amplifier may then be represented as

$$A_1'' = 4\sqrt{I_0 I/N}J_1(z)\sum_n \sin(c_n)\exp\{i(\delta-\pi/2)\} \tag{A6}$$

and

$$A_2'' = 4\sqrt{I_0 I/N}J_2(z)\sum_n \cos(c_n)\exp(2i\delta), \tag{A7}$$

which are digitally squared on a personal computer. The averaged signals are given by

$$\langle A_1''^2\rangle = -8I_0\langle I\rangle J_1^2(z)\exp(2i\delta) \sim -2I_0\langle I\rangle z^2\exp(2i\delta) \tag{A8}$$

for the fundamental harmonic component, and

$$\langle A_2''^2\rangle = 8I_0\langle I\rangle J_2^2(z)\exp(4i\delta) \sim \tfrac{1}{8}I_0\langle I\rangle z^4\exp(4i\delta) \tag{A9}$$

for the second order harmonic component. These signals give $\mu^*(\omega)$ in the same manner as previously written.

In the above procedure, the information on Brownian motion is excluded by squaring the detected signal to yield a sensitive measurement of $\mu^*(\omega)$. In contrast, the diffusion constant of colloidal particles can be obtained separately by eliminating the electrophoretic information. In such a case, the signal A_1 is detected with a lock-in amplifier without employing a squaring operation. If the time constant t_c of the lock-in amplifier is set shorter than the characteristic time of diffusion $1/Dq^2$, it is possible to observe the temporal change of the coefficient $\Sigma_n\sin(c_n)$. By calculating the autocorrelation function of the signal, the diffusion coefficient is obtained from its decay rate.

This method has several advantages when compared to other techniques used in the field of microrheology. First, since lock-in detection removes noise that is asynchronous to the signal, a signal whose amplitude is much smaller than the noise level (by 60 dB) is easily detected. Therefore, both complex electrophoretic mobility and the diffusion constant of colloidal particles in soft materials that scatter light strongly can be measured using this method. Second, the entire signal originally distributed around a harmonic frequency due to Brownian motion is collected with our method. Therefore, the effective intensity of the detected signal is extremely larger than the signal containing the influence of Brownian motion. Third, even if a drifting motion $\delta\mathbf{r}_d(t)=\mathbf{v}_d t$ exists with velocity $\mathbf{v}_d$ in the system studied, the correct complex mobility μ^* can be obtained in our system. That is because Eqs. (A2) and (A3) are not altered if we add the term $\mathbf{q}\cdot\delta\mathbf{r}_d$ to c_n in Eq. (A1), as long as $\mathbf{q}\cdot\mathbf{v}_d$ is smaller than the half-width of a band-pass filter. Therefore, we can apply a higher field to the suspension, which is of great advantage when measuring small displacements at high frequencies.

APPENDIX B: HYDRODYNAMICS OF LYOTROPIC LAMELLAR PHASE

In order to discuss the hydrodynamics of the binary lipid system for large d, we use the phenomenological approach of Brochard and de Gennes [31] for lyotropic smectics. At constant temperature, we need three variables to describe the dynamics of the lamellar phase. These are the total density dilation Θ, the dilation of the layer spacing $\tilde{\gamma}=(d_l-d)/d=\partial u/\partial z$, and the dilation of the surfactant concentration $\tilde{\varepsilon}=(c_0-c)/c_0=\partial c/c_0$, where d_l is the local layer spacing, c_0 is

the prepared surfactant concentration, and c is the local surfactant concentration. Since Θ involves the first sound, which is much faster than the membrane fluctuations we are considering and which yields little effect, we may assume the material is incompressible. One may use the relative change of the area per polar head $\tilde{\delta}=(A-A_{eq})/A_{eq}$ instead of using $\tilde{\varepsilon}$, where A_{eq} is the area per polar head at equilibrium and A denotes its local value. These are related by $\tilde{\varepsilon}=\tilde{\gamma}+\tilde{\delta}$. The free energy density can therefore be expanded as

$$f=\frac{1}{2}B\left(\frac{\partial u}{\partial z}\right)^2+D_{23}\frac{\partial u}{\partial z}\tilde{\delta}+\frac{1}{2}D_{33}\tilde{\delta}^2+\frac{1}{2}K(\nabla_r^2 u)^2$$
$$\equiv f_1+\frac{1}{2}K(\nabla_r^2 u)^2, \tag{B1}$$

where the last term is the membrane curvature elastic energy, and $K=k_c/d$. Following Ref. [32], the equations representing the motion of the fluid are

$$\rho\frac{\partial v_x}{\partial t}=-\frac{\partial p}{\partial x}+\frac{\partial}{\partial x}\left[\frac{\partial f_1}{\partial\tilde{\delta}}\right]_{\tilde{\gamma}}+\eta\left[\frac{\partial^2}{\partial x^2}+\frac{\partial^2}{\partial y^2}+\frac{\partial^2}{\partial z^2}\right]v_x, \tag{B2}$$

$$\rho\frac{\partial v_y}{\partial t}=\frac{\partial p}{\partial y}+\frac{\partial}{\partial y}\left[\frac{\partial f_1}{\partial\tilde{\delta}}\right]_{\tilde{\gamma}}+\eta\left[\frac{\partial^2}{\partial x^2}+\frac{\partial^2}{\partial y^2}+\frac{\partial^2}{\partial z^2}\right]v_y, \tag{B3}$$

$$\rho\frac{\partial v_z}{\partial t}=-\frac{\partial p}{\partial z}+\frac{\partial}{\partial z}\left[\frac{\partial f_1}{\partial\tilde{\gamma}}\right]_{\tilde{\delta}}-K\left(\frac{\partial^4 u}{\partial x^4}+2\frac{\partial^4 u}{\partial x^2\partial y^2}+\frac{\partial^4 u}{\partial y^4}\right)$$
$$+\eta\left[\frac{\partial^2}{\partial x^2}+\frac{\partial^2}{\partial y^2}+\frac{\partial^2}{\partial z^2}\right]v_z, \tag{B4}$$

where p and v represent the local pressure and velocity of the fluid. It is assumed that water does not cross the bilayers and surfactant molecules do not leave the bilayers; that is, there is no permeation. Without permeation, $v_z=\partial u/\partial t$, and the x component of the lipid velocity is given by $v_{Lx}=\partial\tilde{\delta}/\partial t$. Under the conditions of a dilute lamellar phase, it is appropriate to use an isotropic shear viscosity η equal to the viscosity of water in Eqs. (B2)–(B4). However, water may flow between the bilayers in the x direction. This is described by the phenomenological equation [31,32]

$$v_{Lx}-v_x=\mu_s\frac{\partial}{\partial x}\left(\frac{\partial f_1}{\partial\tilde{\delta}}\right)_{\tilde{\gamma}},\quad v_{Ly}-v_y=\mu_s\frac{\partial}{\partial y}\left(\frac{\partial f_1}{\partial\tilde{\delta}}\right)_{\tilde{\gamma}}, \tag{B5}$$

where v_{Lx} and v_{Ly} are the x and y components of the lipid velocity, and μ_s is the slip coefficient, which is estimated as $d^2/12\eta$ [31]. We may then combine $\nabla\cdot\mathbf{v}_L=\partial\tilde{\varepsilon}/\partial t$ with the incompressibility condition $\nabla\cdot\mathbf{v}=0$ to obtain

$$\frac{\partial}{\partial t}(\tilde{\gamma}+\tilde{\delta})=\mu_s\left(\frac{\partial^2}{\partial x^2}+\frac{\partial^2}{\partial y^2}\right)\left(\frac{\partial f_1}{\partial\tilde{\delta}}\right)_{\tilde{\gamma}}. \tag{B6}$$

Equations (B2)–(B4) and (B6) combined with the incompressibility and impermeability conditions form a complete set of equations representing the hydrodynamics of binary lipid systems with large d.

[1] F. C. MacKintosh and C. F. Schmidt, Curr. Opin. Colloid Interface Sci. **4**, 300 (1999).
[2] T. G. Mason and D. A. Weitz, Phys. Rev. Lett. **74**, 1250 (1995).
[3] J. C. Crocker, M. T. Valentine, E. R. Weeks, T. Gisler, P. D. Kaplan, A. G. Yodh, and D. A. Weitz, Phys. Rev. Lett. **85**, 888 (2000).
[4] T. G. Mason, K. Ganesan, J. H. van Zanten, D. Wirtz, and S. C. Kuo, Phys. Rev. Lett. **79**, 3282 (1997).
[5] F. Gittes, B. Schnurr, P. D. Olmsted, F. C. MacKintosh, and C. F. Schmidt, Phys. Rev. Lett. **79**, 3286 (1997).
[6] B. Schnurr, F. Gittes, F. C. MacKintosh, and C. F. Schmidt, Macromolecules **30**, 7781 (1997).
[7] D. Mizuno, Y. Kimura, and R. Hayakawa (unpublished).
[8] D. Mizuno, Y. Kimura, and R. Hayakawa, Langmuir **16**, 9547 (2000).
[9] D. Mizuno, Y. Kimura, and R. Hayakawa, Jpn. J. Appl. Phys., Part 2 **39**, 1197 (2000).
[10] *Micells, Membranes, Microemulsions and Monolayers*, edited by W. M. Gelbart, A. Ben-Shaul, and D. Roux (Springer-Verlag, New York, 1994).
[11] D. Mizuno, Y. Kimura, and R. Hayakawa, Phys. Rev. Lett. **87**, 088104 (2001).
[12] D. Mizuno, T. Nishino, Y. Kimura, and R. Hayakawa, Phys. Rev. E **67**, 061505 (2003).
[13] P. Sens, M. S. Turner, and P. Pincus, Phys. Rev. E **55**, 4394 (1997).
[14] S. D. Druger, M. A. Ratner, and A. Nitzan, Phys. Rev. B **31**, 3939 (1985).
[15] K. S. Schmitz, *An Introduction to Dynamic Light Scattering by Macromolecules* (Academic, San Diego, 1990).
[16] D. Mizuno, K. Hattori, N. Sakamoto, K. Sakai, and K. Takagi, Langmuir **16**, 643 (2000).
[17] H. Scher and M. Lax, Phys. Rev. **109**, 1921 (1958).
[18] É. Freyssingeas, F. Nallet, and D. Roux, Langmuir **12**, 6028 (1996).
[19] M. Jonströmer and R. Strey, J. Phys. Chem. **96**, 5993 (1992).
[20] H. Tanaka, M. Isobe, and J. Yamamoto, Phys. Rev. Lett. **89**, 168303 (2002).
[21] G. Salamat and E. W. Kaler, Langmuir **15**, 5414 (1999).
[22] R. Lipowsky and B. Zielinska, Phys. Rev. Lett. **62**, 1572 (1989).
[23] C. R. Safinya, E. B. Sirota, D. Roux, and G. S. Smith, Phys. Rev. Lett. **62**, 1134 (1989).
[24] J. Happel and H. Brenner, *Low Reynolds Number Hydrodynamics* (Kluwer, Dordrecht, 1991).

[25] S. G. J. M. Kluijtmans, J. K. G. Dhont, and A. P. Philipse, Langmuir **13**, 4982 (1997).
[26] R. Messager, P. Basserea, and G. Porte, J. Phys. (France) **51**, 1329 (1990).
[27] P. G. de Gennes and J. Prost, *The Physics of Liquid Crystals*, 2nd ed. (Oxford University Press, New York, 1993).
[28] T. Imae, T. Iwamoto, G. Platz, and C. Thunig, Colloid Polym. Sci. **269**, 727 (1991).
[29] H. Hoffmann, U. Munkert, C. Thunig, and M. Valiente, J. Colloid Interface Sci. **163**, 217 (1994).
[30] Y. Iwashita and H. Tanaka, Phys. Rev. Lett. **90**, 045501 (2003).
[31] F. Brochard and P. G. de Gennes, Pramana, Suppl. **1**, 1 (1975).
[32] C. Y. Zhang, S. Sprunt, and J. D. Litster, Phys. Rev. E **48**, 2850 (1993).
[33] D. Mizuno, T. Nishino, Y. Kimura, and R. Hayakawa (unpublished).